Energy Storage Materials xxx (xxxx) xxx–xxx

Contents lists available at ScienceDirect

Energy Storage Materials

journal homepage: www.elsevier.com/locate/ensm

High air-stability and superior lithium ion conduction of $Li_{3+3x}P_{1-x}Zn_xS_{4-x}O_x$ by aliovalent substitution of ZnO for all-solid-state lithium batteries

Gaozhan Liu[a,b,1], Dongjiu Xie[a,1], Xuelong Wang[b,c], Xiayin Yao[a], Shaojie Chen[a,*], Ruijuan Xiao[c,*], Hong Li[c], Xiaoxiong Xu[a]

[a] Ningbo Institute of Materials Technology & Engineering, Chinese Academy of Sciences, 315201 Ningbo, PR China
[b] University of Chinese Academy of Sciences, 100049 Beijing, PR China
[c] Institute of Physics, Chinese Academy of Sciences, 100190 Beijing, PR China

ARTICLE INFO

Keywords:
aliovalent substitution
high air-stability
superior lithium ion conductivity
theoretical calculation
all-solid-state lithium battery

ABSTRACT

A series of new solid electrolytes of $Li_{3+3x}P_{1-x}Zn_xS_{4-x}O_x$ (x = 0.01, 0.02, 0.03, 0.04, 0.05, 0.06) are synthesized successfully via Zn, O co-doping the Li_3PS_4 glass-ceramic for the first time. The result shows that Li_3PS_4 aliovalent substitution of 2 mol% ZnO ($Li_{3.06}P_{0.98}Zn_{0.02}S_{3.98}O_{0.02}$) presents the highest conductivity of 1.12×10^{-3} S cm^{-1} at room temperature, which is twice that of the pristine Li_3PS_4. Besides, $Li_{3.06}P_{0.98}Zn_{0.02}S_{3.98}O_{0.02}$ exhibits excellent stability against humid air, lithium metal and chlorobenzene solvent. The mechanisms of the enhancement of conductivity and air-stability are well understood by conducting first-principles density functional theory (DFT) calculation and Bond-Valence (BV) analysis, and the results well demonstrate that the conductivity and air-stability of Li_3PS_4 could be improved via Zn, O dual-doping, in which partial P^{5+} could be substituted by Zn^{2+}, and a part of S^{2-} could be replaced by O^{2-}. Finally, the all-solid-state lithium battery (ASSLB) with bi-layer electrolytes of $LiCoO_2/Li_{10}GeP_2S_{12}/Li_{3.06}P_{0.98}Zn_{0.02}S_{3.98}O_{0.02}$/Li is assembled, and it delivers an initial discharge capacity of 139.1 mAh g^{-1} at 0.1 C and a capacity retention of 81.0% after 100 cycles at room temperature. This work combines systematical experimental characterizations and sufficient theoretical calculations to develop a new promising sulfide electrolyte with superior lithium ion conductivity and high air-stability for ASSLBs application.

1. Introduction

All-solid-state lithium batteries (ASSLBs) are attracting interest at an exponentially increasing pace due to the possibility of replacing conventional lithium ion batteries (LIBs) as the next generation energy storage systems [1]. This novel battery might settle the safety concerns that LIBs currently meet, most importantly, the energy density of ASSLBs could be further improved by using lithium metal as anode, making it a promising candidate for large scale energy storage devices such as cell phones, electric vehicles and smart grid, etc. However, several challenges are still need to be overcome in ASSLBs for their successful commercialization in real applications. It is well known that solid electrolytes (SEs) as the core component of ASSLBs could be classified into three types, that is, polymer electrolytes, inorganic electrolytes and organic-inorganic composite electrolytes [2–4]. Normally, inorganic electrolytes could be further divided into oxide electrolytes and sulfide electrolytes. The oxide electrolytes are usually stable in air, but most of their lithium ionic conductivities are in the order of 10^{-4} S cm^{-1} at room temperature and with insufficient interface contact between electrolyte/electrode such as garnets and NASICONs [5,6]. The sulfide electrolytes possess higher conductivities from 10^{-4} to 10^{-2} S cm^{-1} at room temperature owing to the larger ionic radii and weaker electronegativity of sulfide ions [1,7–9]. The highest conductivity was found in the $Li_{9.54}Si_{1.74}P_{1.44}S_{11.7}Cl_{0.3}$ (25 mS cm^{-1} at 25 °C), which is comparable to that of conventional organic liquid electrolytes [1]. Besides, sulfide electrolytes have wide electrochemical windows and negligible electronic conductivities, which are of great importance from the perspective of applying in ASSLBs [10]. Especially, the grain-boundary resistance of sulfide electrolytes can be largely decreased by cold pressing at room temperature even without a high-temperature sintering process [11]. This mechanical property of sulfide electrolytes is suitable for forming a favorable solid-solid contact at the electrode/electrolyte interface in ASSLBs, which could greatly improve the cycle performance. However, the sensitivity of sulfide electrolytes against moisture in air seriously restricts their large scale applications. Additionally, some of sulfide electrolytes contain Ti, Ge, and other

* Corresponding authors.
E-mail addresses: chenshaojie@nimte.ac.cn (S. Chen), rjxiao@iphy.ac.cn (R. Xiao).
[1] Gaozhan Liu and Dongjiu Xie contributed equally to this work.

https://doi.org/10.1016/j.ensm.2018.07.008
Received 2 May 2018; Received in revised form 6 July 2018; Accepted 10 July 2018

valence-variable elements, which are not stable when they are contacted with Li anode. Consequently, the researchers in the world still devote themselves to the development of an "ideal" SE, which can present high conductivity, wide electrochemical window, good chemical stability against solvents and lithium metal as well as stable in air. Remarkably, Kanno et al. have developed a series of sulfide crystals with *thio*-LISICON structure, in which the conduction pathways in the lattice possess suitable size for the migration of mobile ions while the sublattice is in disorder, and the mobile ions and anion sublattices are highly polarizable, thus this structure has improved mobility of the conducting species [9,12–14]. Among these *thio*-LISICON crystals, the sulfide electrolyte Li_3PS_4 has been widely studied in recent years, which is ascribed to its relative high conductivity above 10^{-4} S cm^{-1} and good compatibility with Li. Furthermore, Li_3PS_4 can be synthesized at low temperature and possesses good processability. Most importantly, the Li_3PS_4 glass and glass-ceramic composed of Li^+ and PS_4^{3-} ions present the most stability in air and generate the least amount of H_2S among the Li_2S-P_2S_5 binary system [15]. Nevertheless, although Li_3PS_4 presents the relative high conductivity (10^{-4} S cm^{-1} at room temperature) and stability in air, the finite ionic conductivity and insufficient air-stability of Li_3PS_4 still hinder its applications in ASSLBs on a large scale. Therefore, researchers tried various approaches to further improve its conductivity and stability [1,11,16].

It is reported that doping with oxides, such as Li_2O [17,18], Li_2ZrO_3 [19], P_2O_5 [20–23] and Li_3PO_4 [24] into (100-x)Li_2S-xP_2S_5 can improve their chemical stabilities and conductivities. In our previous work, P_2O_5 was chosen to doping Li_3PS_4, using O^{2-} to partially replace S^{2-} in order to enhance its conductivity and stability. After the substitution, a non-bridging sulfur atom could be substituted with a bridging oxygen atom, leading to the formation of a weaker trap for lithium ions and the lower activation energy for lithium ion migration, and the lithium ion conductivity is improved to 8×10^{-4} S cm^{-1} at room temperature[23]. In addition, the larger Se^{2-} in the chalcogens was selected for doping in 75Li_2S-(25-x)P_2S_5-xP_2Se_5 [25]. It was found that for both amorphous and crystalline electrolytes, the ionic conductivities were enhanced with an increased Se content, and the crystalline electrolyte with 2 mol% of P_2Se_5 exhibited the highest conductivity of 6×10^{-4} S cm^{-1} at room temperature.

Additionally, as mentioned above, although sulfide electrolytes are competent candidates as SEs for ASSLBs [4,9], the handling of sulfide electrolytes must be done in an inert gas atmosphere because the hydrolyses of the sulfides would cause structural changes and generate H_2S gas in air [15]. Therefore, air-stability is another bottle-neck for the sulfide electrolytes commercialization. Akitoshi Hayashi et al. decreased the release amount of H_2S via adding Fe_2O_3 or Bi_2O_3 nanoparticles into Li_3PS_4 electrolytes, and proposed that the use of a favorable nanoparticle with a larger negative Gibbs energy change (ΔG) for reacting with H_2S was effective in decreasing the H_2S amount [10]. Alternatively, Sahu et al. reported the design of aliovalent substitution of Li_4SnS_4 to achieve high conduction and excellent air-stability based on the hard and soft acids and basestheory [26]. Besides, Ohtomo et al. revealed that the addition of Li_2O could effectively reduce the amount of generated H_2S. Moreover, they found that the existence of Li_2S was the cause of H_2S generation, while less Li_2S content led to superior stability in air [27].

Herein, ZnO was selected to aliovalent substitution of the Li_3PS_4 structure according to the result of theoretical calculation by the first time to our knowledge, in which partial P^{5+} could be substituted by Zn^{2+}, and a part of S^{2-} could be replaced by O^{2-}. The synthesis parameters of Zn, O dual-doped Li_3PS_4 sulfides have been systematically studied. Conductivities and crystal structures depending on added ZnO amount were analyzed via X-ray diffraction (XRD), electrochemical impedance spectroscopy (EIS), and theoretical calculations. In particular, the suppression of H_2S gas was investigated, and the H_2S gas generation from the obtained ZnO doped Li_3PS_4 sulfide was discussed as well. The mechanisms of conductivity and air-stability improvement are well understood by conducting first-principles density functional theory (DFT) calculation and Bond-Valence (BV) analysis. Moreover, the stability in organic solvent of the prepared glass-ceramic was also characterized. Finally, the optimal synthesized sulfide electrolyte was applied in the construction of ASSLB with bi-layer electrolytes, $LiCoO_2$/bi-layer SEs/Li, and the charge-discharge performance of the battery was examined.

2. Experimental

2.1. Theoretical method

The DFT calculations performed in this study are carried out with the Vienna ab initio simulation package (VASP) within the projector augmented-wave (PAW) approach [28,29]. The generalized gradient approximation in the parameterization of Perdew, Burke, and Ernzerhof (PBE) is adopted to describe the exchange–correlation functional [30]. For all calculations the cut-off energy of wave function are 500 eV. For the convenience of building β-Li_3PS_4 model structure, supercells containing 16 and 48 formula units (f.u.) of Li_3PS_4 are used to simulate $Li_{3+3x}P_{1-x}Zn_xS_{4-x}O_x$ with x = 0.021 and x = 0.0625. One P atom and one S atom in the supercell are replaced by Zn atom and O atom respectively. Three extra Li atoms are added to the supercell occupying 4c sites to maintain electronic neutrality. The 30 configurations with lowest electrostatic energy are chosen to conduct DFT based optimization and total energy calculation. The structure with lowest DFT total energy is considered as groundstate structure. For all DFT calculations only gamma point in Brillouin zone is used on account of the large supercell we use. For the relaxations of supercells, the forces felt by each of the atoms are well converged below 0.05 eV Å^{-1}. The BV method is employed to obtain the Li migration pathways [31]. Furthermore, the XRD pattern for $Li_{3+3x}P_{1-x}Zn_xS_{4-x}O_x$ with x = 0.021 is simulated at Cu Kα radiation wavelength (0.154 nm) with VESTA software [32].

2.2. Preparation method

P_2S_5 (99%, Aladdin Chemistry. Co., Ltd.), Li_2S (99.9%, Sigma-Aldrich) and ZnO (99.9%, Aladdin Chemistry. Co., Ltd.) were used as starting materials to prepare $Li_{3+3x}P_{1-x}Zn_xS_{4-x}O_x$ amorphous powders through high-energy ball-milling. A planetary ball mill apparatus (Retch, PM400) including a 50 ml zirconia pot with 50 zirconia balls was used to perform ball-milling. The milling speed and time were 500 rpm and 12, 13.5, 15 hours (h), respectively. The amorphous powders were heated at 230 ~ 270 °C for 3 ~ 5 h to obtain the $Li_{3+3x}P_{1-x}Zn_xS_{4-x}O_x$ (x = 0, 0.01, 0.02, 0.03, 0.04, 0.05, 0.06) glass-ceramics.

In contrast, P_2S_5 (99%, Aladdin Chemistry. Co., Ltd.) and Li_2S (99.9%, Sigma-Aldrich) were used to prepare amorphous Li_3PS_4 through high-energy ball-milling. Then, ZnO (99.9%, Aladdin Chemistry. Co., Ltd.) was added to amorphous Li_3PS_4 and heated at 250 °C for 4 h to obtain the mixture of 0.98 Li_3PS_4·0.02 ZnO.

All preparation processes were carried out in an argon-filled glove box with H_2O < 0.1 ppm and O_2 < 0.5 ppm (Lab Star, Mbraun, Germany).

$Li_{10}GeP_2S_{12}$ (LGPS) with the Li^+ conductivity of 6.22 × 10^{-3} S cm^{-2} at 25 °C prepared by solid-state reaction method which can be found in some early reports [33] was used as the one of bi-layer electrolytes for the assembly of ASSLBs. The $LiCoO_2$ material was prepared by solid state method. In a typical synthesis process, the Co_3O_4 and Li_2CO_3 (99.9%, Aladdin Chemistry. Co., Ltd.) were ball-milled in the mortar with a molar ratio of 2/3 for 4 h, followed by a sintering procedure at 850 °C for 20 h, and the as-prepared product was grinded again to obtain a fine powder. Afterward, the $LiCoO_2$ particles was coated with $LiNbO_3$ by the sol-gel method [34,35].

2.3. Characterization and instruments

XRD measurements were performed on a Bruker AXS D8 Advance with Cu Kα radiation (λ = 1.5406 Å). The diffraction data was collected in a 2θ range from 10° to 80°. Scanning electron microscope (SEM, S4800, Hitachi) Microstructure and element mapping was performed on a transmission electron microscope (TEM, Tecnai G2 F20, FEI). Via-reflex Raman spectrophotometer with a Renishaw was employed to record the Raman spectra by using the 532 nm line. Ionic conductivities were characterized for the cold pressed samples at 300 MPa with 10 mm of diameter and ~1.2 mm of thickness by alternating current (AC) impedance method and carbon plates were selected as blocking electrodes on both sides of the pellets. EIS was performed on an impedance analyzer (Solartron, 1470E) at frequencies from 1 MHz to 10 Hz in an argon atmosphere over a temperature range of -40 °C ~100 °C. The galvanostatic charge-discharge cycling of the symmetric anode/ $Li_{3.06}P_{0.98}Zn_{0.02}S_{3.98}O_{0.02}$/anode cell was carried out on a standard battery test instrument (Wuhan Rambo Electronics Co., Ltd.) at 0.5 mA cm^{-1}, 25 °C.

The amount of H_2S gas generated from the obtained samples were measured. Pelletized samples (100 mg), a H_2S gas sensor (GX-2009, Riken Keiki Co., Ltd., Tokyo), and a fan were placed in a sealed container filled with humid air. The volume of the container is 1750 cm^3. The amount of H_2S gas generated from the sample was calculated from the H_2S concentration measured by the H_2S gas sensor. The temperature was set to 30 °C and the relative humidity was kept at 55% during the measurement.

The stability of the prepared sulfide electrolyte in chlorobenzene solvent was characterized as well. Preparation of slurry of 1:1 by volume of SE and chlorobenzene, then, dry the slurry after a certain time (1 min, 120 min or 24 h), and test their conductivities before/after soaking. All these procedures performed in Ar ambience.

2.4. All-solid-state lithium battery assembly

$LiNbO_3$-coated $LiCoO_2$ was used as cathode material [36]. The composite of $LiNbO_3$-coated $LiCoO_2$ and LGPS at a weight ratio of 7:3 were uniformly mixed as the working electrode. Metallic Li was selected as anode. As for the SE layer, the bi-layer electrolytes was obtained by sequential pressing electrolytes of LGPS and $Li_{3.06}P_{0.98}Zn_{0.02}S_{3.98}O_{0.02}$ ($Li_{3+3x}P_{1-x}Zn_xS_{4-x}O_x$, x = 0.02) under 240 MPa. The thickness of the bi-layer electrolytes after press is about 1 mm. Afterwards, the composite cathode was uniformly spread on the side of LGPS layer and pressed under 240 MPa, and the Li foil (99.9%, Alfa Aesar) was attached to the side of $Li_{3.06}P_{0.98}Zn_{0.02}S_{3.98}O_{0.02}$ by pressing under 180 MPa. The assembled ASSLBs were charged and discharged in galvanostatic mode at 0.1 C (1 C = 120 mAh g^{-1}) in the range of 3.0-4.3 V *vs* Li/Li^+. The whole process was performed in an argon-filled glove box. As a contrast, the $LiCoO_2$/LGPS/Li_3PS_4/Li cell was assembled as well. Fig. 1 schematic illustrates the structure of ASSLB $LiCoO_2$/LGPS/$Li_{3.06}P_{0.98}Zn_{0.02}S_{3.98}O_{0.02}$ /Li.

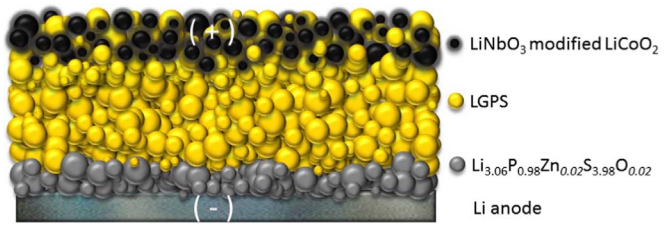

Fig. 1. Schematic diagram of the $LiCoO_2$/LGPS/ $Li_{3.06}P_{0.98}Zn_{0.02}S_{3.98}O_{0.02}$ /Li all solid-state cell.

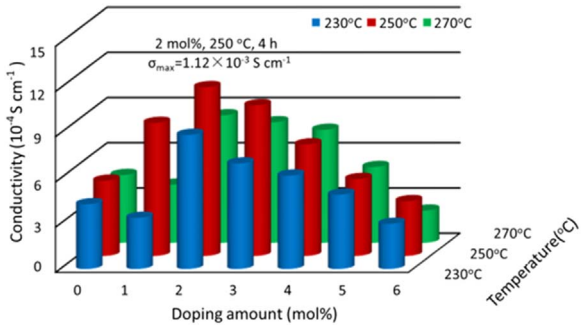

Fig. 2. Conductivities of $Li_{3+3x}P_{1-x}Zn_xS_{4-x}O_x$ (x = 0, 0.01, 0.02, 0.03, 0.04, 0.05, 0.06) glass-ceramics with different annealing conditions.

3. Results and discussion

3.1. Optimized preparation of $Li_{3+3x}P_{1-x}Zn_xS_{4-x}O_x$ (x = 0 ~ 0.06) glass-ceramics

The $Li_{3+3x}P_{1-x}Zn_xS_{4-x}O_x$ (x = 0, 0.01, 0.02, 0.03, 0.04, 0.05, 0.06) glass-ceramics were prepared by using the mechanical milling technique and subsequently annealing process [37]. Experimental parameters including doping amount of ZnO, time of ball-milling, and the temperature and time of annealing process were examined one by one as presented in Fig. S1 (Supporting Information). Finally, $Li_{3.06}P_{0.98}Zn_{0.02}S_{3.98}O_{0.02}$ ($Li_{3+3x}P_{1-x}Zn_xS_{4-x}O_x$, x = 0.02) with the favorable ingredient proportion exhibits the highest ionic conductivity of 1.12×10^{-3} S cm^{-1} at room temperature after ball-milling for 13.5 h and then annealed at 250 °C for 4 h. Fig. 2 summarized the different conductivities of the synthesized electrolytes under different synthesis conductions.

3.2. X-ray diffraction

XRD patterns were performed to analyze the phase compositions of $Li_{3+3x}P_{1-x}Zn_xS_{4-x}O_x$ electrolyte with different ZnO amount, as shown in Fig. 3, multiple crystallization peaks were observed, suggesting the formation of glass-ceramics. It is worth noting that peaks of ZnO could be found in the sample of $0.98Li_3PS_4{\cdot}0.02ZnO$, while only characteristic peaks of β-Li_3PS_4 phase could be found in $Li_{3.06}P_{0.98}Zn_{0.02}S_{3.98}O_{0.02}$ without ZnO peaks, indicating that ZnO is dual doped into the crystal structure rather than just physical mixing. The apexes of the PS_4^{3-} tetrahedrons are still arranged in a zig-zag manner, and there are two sites for lithium ions, both in the octahedral and tetrahedral sites [38]. As a result, these ion partitions could facilitate the migration of the interstitial lithium ions.

When x = 0.06, the intensity of crystallization peaks corresponding to β-Li_3PS_4 decreased significantly and crystallization peaks of thio-LISICON II analog [39] emerged, which suggested that large amount of

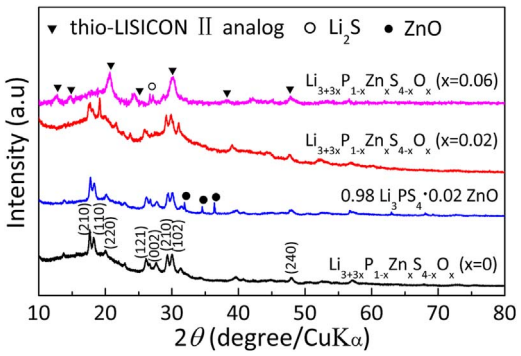

Fig. 3. The XRD patterns of $Li_{3+3x}P_{1-x}Zn_xS_{4-x}O_x$ (x = 0, 0.02, 0.06) and $0.98Li_3PS_4{\cdot}0.02ZnO$.

ZnO doping obviously changed the crystal structure of β-Li_3PS_4. Notably, no ZnO characteristic peaks could be observed in either x = 0.02 or x = 0.06 sample, indicating that both Zn and O atoms have been doped into the Li_3PS_4 crystal structure, instead of existing as the third phase, which could be further supported by the theoretical calculation. The energy change ΔE for the following hypothetical reaction (1) is calculated:

$$(1-x)Li_3PS_4 + 3xLi_2S + xZnO \rightarrow Li_{3+3x}P_{1-x}Zn_xS_{4-x}O_x \quad (1)$$

For x = 0.021, the ΔE is 3.9 meV/atom, while for x = 0.0625, the ΔE is 5.2 meV/atom. ΔE being positive indicates that it is actually energetically unfavorable for ZnO to solute into crystalline β-Li_3PS_4. However, a small ΔE suggests small driving force for ZnO doped β-Li_3PS_4 to decompose into ZnO and β-Li_3PS_4 phase. The Zn and O dopants can be easily stabilized by some defects or entropic factor. The results could also help explain why the synthesized SE stays in glass-ceramic form. The reduced domain size of crystalline phase and enormous structural defects in glass phase are beneficial to stabilizing the Zn and O dopants. Furthermore, ΔE is bigger for x = 0.0625 than that for x = 0.021, which means that ZnO doped β-Li_3PS_4 phase is more unstable when x is bigger. The change of crystallization peaks in XRD spectra for x = 0.06 is consistent with the calculation results.

The comparison of the simulated and experimental XRD patterns obtained through calculation and characterization are shown in Fig. 4(a). From the XRD pattern comparison, the two XRD patterns are nearly identical, suggesting that the obtained material is $Li_{3.06}P_{0.98}Zn_{0.02}S_{3.98}O_{0.02}$, in which P^{5+} and S^{2-} were partially replaced by Zn^{2+} and O^{2-}, respectively. No peaks related to impurity are observed within the figure. However, slight differences between the XRD patterns could be observed at 2θ of 27-30° which is attributed to the lattice parameter obtained by DFT calculation is deviated from the experimental values. The 4b sites are set being fully occupied by Li ions in DFT simulation while only around 70% of 4b sites are actually occupied in β-Li_3PS_4 which causes that the calculated a and c is bigger while b is smaller than the experimental values [40,41]. The optimized supercell structure of $Li_{3.06}P_{0.98}Zn_{0.02}S_{3.98}O_{0.02}$ is shown in Fig. 4(b). As can be seen, the crystal framework of ZnO doped β-Li_3PS_4 is the same with β-Li_3PS_4 consisting of isolated PS_4 tetrahedron arranged in a zig-zag layer and connected with edge-shared LiS_6 octahedron. The ZnS_4 tetrahedron is bigger than the PS_4 tetrahedron and the O dopant is in the adjacent PS_4 unit. It's worth pointed out that more Li ions are clearly displaced towards the ZnS_4 tetrahedron which could be driven by electrostatic attraction between Li^+ ions and highly negative charged ZnS_4^{6-} unit.

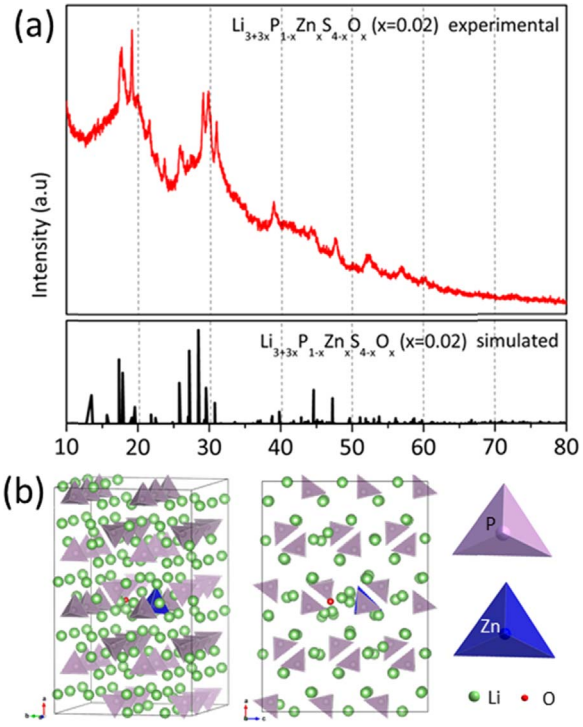

Fig. 4. (a) Experimental and simulated XRD patterns of $Li_{3+3x}P_{1-x}Zn_xS_{4-x}O_x$ (x = 0.02); (b) structure of $Li_{3+3x}P_{1-x}Zn_xS_{4-x}O_x$ (x = 0.02) from DFT calculations.

3.3. Electron microscope

Fig. 5(a) shows the morphologies of pristine Li_3PS_4, and Fig. 5(b) is the morphologies of $Li_{3.06}P_{0.98}Zn_{0.02}S_{3.98}O_{0.02}$ particles. Comparing with pristine Li_3PS_4, the $Li_{3.06}P_{0.98}Zn_{0.02}S_{3.98}O_{0.02}$ particles are similar, and no apparent differences could be found. Besides, it could be also found that the sizes of $Li_{3.06}P_{0.98}Zn_{0.02}S_{3.98}O_{0.02}$ particles are range in 1~4 μm with irregular morphologies. As revealed by the TEM (Fig. 5c), the smallest size of $Li_{3.06}P_{0.98}Zn_{0.02}S_{3.98}O_{0.02}$ electrolyte particles is around 1μm. The high resolution transmission electron microscope (HRTEM) image in Fig. 5(d) shows clear lattices with interplanar distance of 0.298 nm, matching well with the d_{210} spacing of $Li_{3.06}P_{0.98}Zn_{0.02}S_{3.98}O_{0.02}$ electrolyte. Furthermore, the scanning transmission electron microscopy-energy dispersive spectrometer (STEM-EDS) elemental mapping of $Li_{3.06}P_{0.98}Zn_{0.02}S_{3.98}O_{0.02}$ in Fig. 5(e) also confirms that the $Li_{3.06}P_{0.98}Zn_{0.02}S_{3.98}O_{0.02}$ contain phosphorus, sulfur, zinc and oxygen in nano scale, and all elements are homogeneously distributed throughout the particles, which is proved that zinc and oxygen is doped into Li_3PS_4 again.

3.4. Conductivities and activation energy

The conductivities were measured every 10 °C from -40 °C to 100 °C [42], and the results are shown in Fig. 6. The conductivities of all samples increasing as the temperature increase. Obviously, the sample with x = 0.02 shows the highest conductivity among these ZnO doped electrolytes. The conductivities of x = 0.02 at -40 °C and 0 °C are still as high as 3.10×10^{-5} S cm^{-1} and 1.94×10^{-4} S cm^{-1}, respectively. At room temperature, the conductivity is above 10^{-3} S cm^{-1}. Furthermore, their activation energies (E_a) could be calculated according to the Eq. (2),

$$\sigma = A\exp\left(-\frac{Ea}{RT}\right) \quad (2)$$

Where, σ = ionic conductivity; A = pre-exponential factor; E_a = activation energy; R = gas constant; T = absolute temperature, K.

$Li_{3.06}P_{0.98}Zn_{0.02}S_{3.98}O_{0.02}$ shows the smallest value of 29.787 kJ mol^{-1} among these samples, while the E_a of x = 0.06 presents the largest value of 32.311 kJ mol^{-1}. In order to understand why E_a for Li^+ migration is the smallest when x = 0.02, we investigate the atomic configurations and Li^+ migration pathways of $Li_{3+3x}P_{1-x}Zn_xS_{4-x}O_x$ models with x = 0.021 and x = 0.0625 by conducting DFT calculation and BV analysis [43]. Through the difference in the Li^+ migration pathways between models solely doped with Zn and co-doped with Zn/O, a synergetic effect of Zn-O co-doping is found for x = 0.021. As shown in Fig. 7, the migration pathways of Li^+ ions are indicated by the isosurface of potential energies. With the low dopants concentration of 0.021 and 0.0625, the continuous migration channels are still in the ***b*-*c*** plane implying a 2D transportation behavior of Li^+ ions like in Li_3PS_4 [41]. When Zn dopant is introduced to P site as the situation shown in Figs. 7a and 6b, the pathways of Li^+ ions vanished around Zn dopant for both x = 0.021 and x = 0.0625. This result suggests that single Zn dopant would hinder the migration of Li^+ ions around itself. When O dopant is further introduced as the situation shown in Figs. 7c and 6d, the migration channels of Li^+ ions around O dopant are enlarged for both x = 0.021 and x = 0.0625, which is similar with the P_2O_5 doped Li_3PS_4. The difference between Zn dopant and O dopant is very likely due to the different bond lengths (Supporting Information

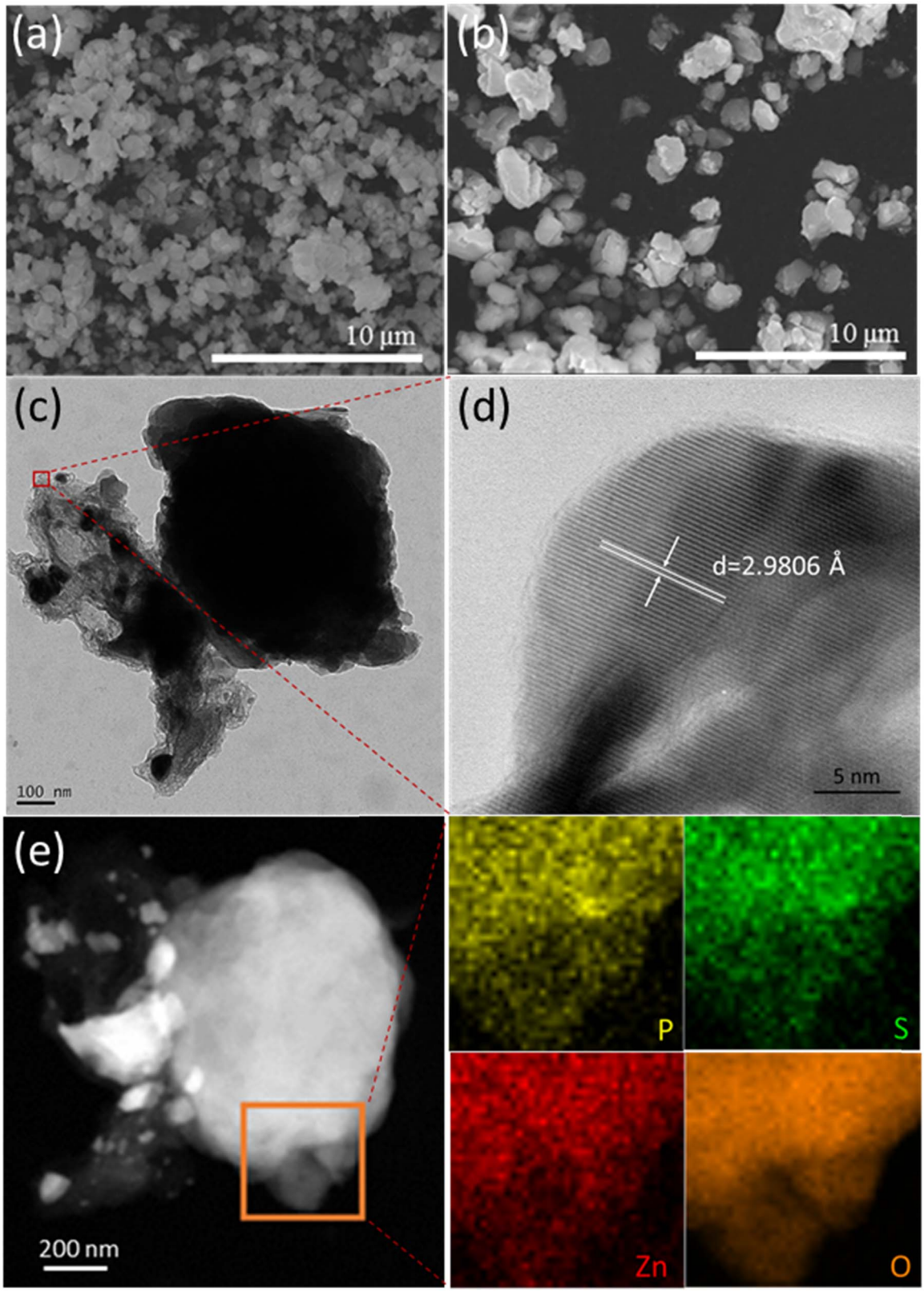

Fig. 5. The SEM images of (a) Li_3PS_4, (b) $Li_{3.06}P_{0.98}Zn_{0.02}S_{3.98}O_{0.02}$,the (c) TEM, and (d) HRTEM images, and (e) STEM EDS elemental mapping images of $Li_{3.06}P_{0.98}Zn_{0.02}S_{3.98}O_{0.02}$, marked by the rectangle region, for P, S, Zn and O.

Table S1). Zn-S bond is much longer than P-O bond which would decrease the free space for Li^+ traveling through. However, for the case of x = 0.021, O dopant prefers appearing in the neighbor of Zn dopant and synergistically enlarges the migration channel for Li^+ around Zn. In contrast, with x = 0.0625 the O dopant would rather stay far from the Zn dopant and the hindered Li^+ migrating situation around Zn does not improve. In addition, in model with x = 0.0625 the average volume taken by single PS_4 tetrahedron unit is smaller than that in undoped Li_3PS_4 which will lead to the crystal structure varied as shown in Fig. 3, while for x = 0.021 the volume stays the same. This shrink in unit cell

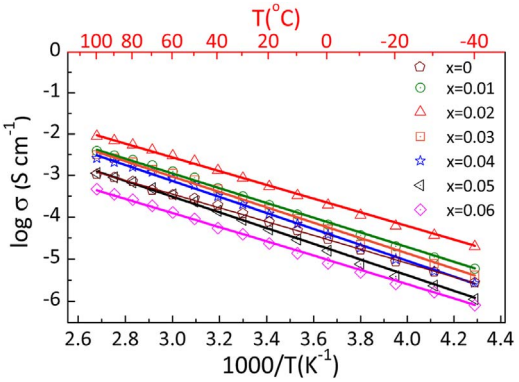

Fig. 6. Arrhenius plots of $Li_{3+3x}P_{1-x}Zn_xS_{4-x}O_x$ (x = 0, 0.01, 0.02, 0.03, 0.04, 0.05, 0.06).

volume would increase E_a since it reduces the free space for Li^+ ions to move through. Though small amount of O doping benefits Li^+ ions migration in Li_3PS_4, short P-O bonds and small O^{2-} ions would cause shrink of the unit cell volume, which is a disadvantage for fast ionic conduction. However, in $Li_{3.06}P_{0.98}Zn_{0.02}S_{3.98}O_{0.02}$, since O stays near to Zn, long Zn-S bond and big ZnS_4 tetrahedron could counteract with PS_3O unit and minimize the shrinkage of unit cell, which is consistent with the XRD results in the Fig. 3. Furthermore, we calculate the energy change ΔE for the following hypothetical reaction (3):

$$Li_3PS_{4-x}O_x + Li_{3(1+x)}P_{1-x}Zn_xS_4 \rightarrow Li_{3(1+x)}P_{1-x}Zn_xS_{4-x}O_x + Li_3PS_4 \quad (3)$$

To study whether it's energetically favorable for Zn and O dopants to stay together spatially. For x = 0.021, ΔE is -0.5 meV/atom, while ΔE

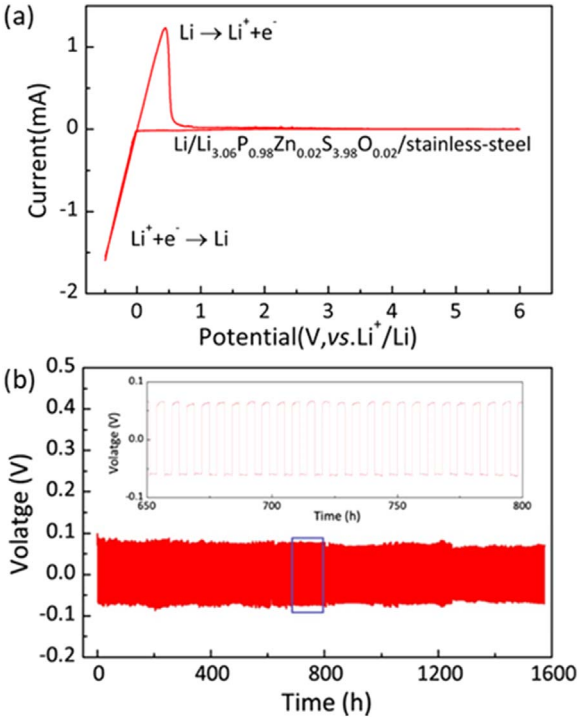

Fig. 8. (a) The Cyclic Voltammetry of $Li_{3.06}P_{0.98}Zn_{0.02}S_{3.98}O_{0.02}$ from -0.5 to 6 V *vs.* Li/Li^+; (b) Galvanostatic cycling of the symmetric anode/ $Li_{3.06}P_{0.98}Zn_{0.02}S_{3.98}O_{0.02}$/anode cell.

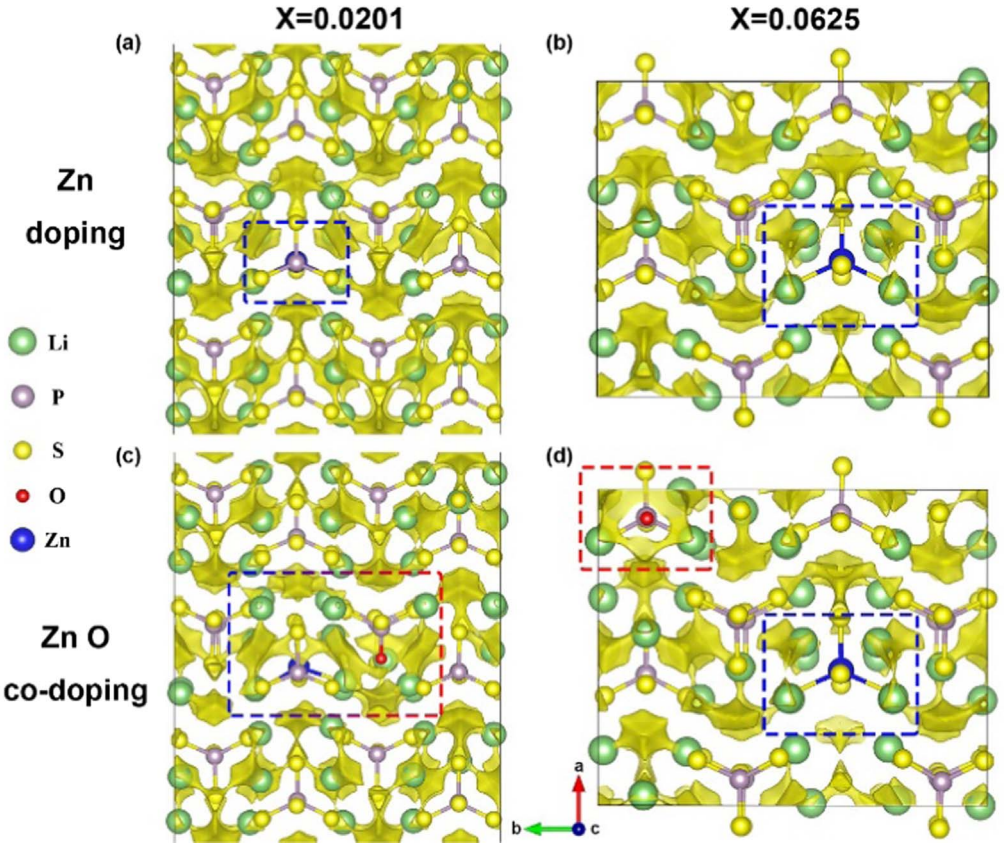

Fig. 7. The Li^+ ions migration pathways by BV analysis for β-Li_3PS_4 solely doped with Zn (a and b) and co-doped with Zn and O (c and d). (a) and (c) are for dopants concentration x = 0.021. b and d are for x = 0.0625. The green, grey, yellow, red and blue spheres represent Li, P, S, O and Zn atomic sites, respectively. The space enclosed by the light yellow isosurface indicates the Li^+ migration pathway. The local pathways around Zn and O dopants are marked by blue and red dashed line boxes respectively.

is 1.15 meV/atom for x = 0.0625. It can be seen that when x = 0.021 Zn and O prefer staying together while they tend to separate when doping content increases. In summary, for $Li_{3.06}P_{0.98}Zn_{0.02}S_{3.98}O_{0.02}$, Zn and O dopants stay close to each other and synergistically minimize the volume shrinkage and promote Li^+ ions migration around themselves. As a result, the E_a of $Li_{3.06}P_{0.98}Zn_{0.02}S_{3.98}O_{0.02}$ is smaller than samples with higher doping contents.

3.5. Electrochemical stability

The electrochemical window of $Li_{3.06}P_{0.98}Zn_{0.02}S_{3.98}O_{0.02}$ was analyzed via cyclic voltammetry (CV) test. The scan rate was 1 mV s^{-1}, and the scan range was from -0.5 V to 6 V *vs.* Li/Li^+. As profiled in Fig. 8a, the result of CV indicates that the reduction and oxidation peak around -0.5 V and 0.5 V are corresponded to the deposition and decomposition of lithium, respectively. No other peaks are detected in the whole scan range, indicating $Li_{3.06}P_{0.98}Zn_{0.02}S_{3.98}O_{0.02}$ is electrochemically stable up to 6 V and possesses a wide electrochemical window.

Additionally, Li/$Li_{3.06}P_{0.98}Zn_{0.02}S_{3.98}O_{0.02}$/Li symmetric cell was assembled to investigate its stability against lithium. Galvanostatic charge-discharge test was conducted on this symmetric cell in order to study the stability with lithium. In the galvanostatic charge-discharge test, the current density was 0.5 mA cm^{-2} at room temperature. The result of galvanostatic charge-discharge test shows that no obvious changes were observed in the symmetric cell (Fig. 8b), proving $Li_{3.06}P_{0.98}Zn_{0.02}S_{3.98}O_{0.02}$ is outstandingly stable against lithium.

3.6. Stability in air and organic solvent

In order to evaluate the stability of $Li_{3.06}P_{0.98}Zn_{0.02}S_{3.98}O_{0.02}$ in ambient environment, $Li_{3.06}P_{0.98}Zn_{0.02}S_{3.98}O_{0.02}$ specimens were exposed in humid air for different amount of time. As well known that H_2S is one of the common products when sulfide electrolytes react with H_2O, the amount of generated H_2S over time was served as the indicator of this reaction. The results suggest that $Li_{3.06}P_{0.98}Zn_{0.02}S_{3.98}O_{0.02}$ hardly react with the H_2O in air as presented in Fig. 9 and the concentration of H_2S is only 0.0175 cm^3 g^{-1} after 180 minutes, while 0.07 cm^3 g^{-1} for Li_3PS_4 after 20 minutes [10]. It could be well explained by the calculation results. To estimate the driving force for sulfide electrolyte reacting with H_2O, we calculate the energy change ΔE for following reaction (4),

$$Li_{3+3x}P_{1-x}Zn_xS_{4-x}O_x + yH_2O \rightarrow Li_{3+3x}P_{1-x}Zn_xS_{4-x-y}O_{x+y} + yH_2S \quad (4)$$

according to the calculated results, for x = 0, ΔE is -912.15 J mol^{-1}, while ΔE is -882.3 J mol^{-1} for x = 0.021. The bigger entropy loss for Li_3PS_4 reacting with H_2O compared to $Li_{3.06}P_{0.98}Zn_{0.02}S_{3.98}O_{0.02}$ indicates that undoped Li_3PS_4 is more easily reacting with H_2O. At the same environmental condition, higher reacting rate is also expected between Li_3PS_4 and H_2O than that between $Li_{3.06}P_{0.98}Zn_{0.02}S_{3.98}O_{0.02}$ and H_2O which will cause producing more H_2S during a certain amount of time.

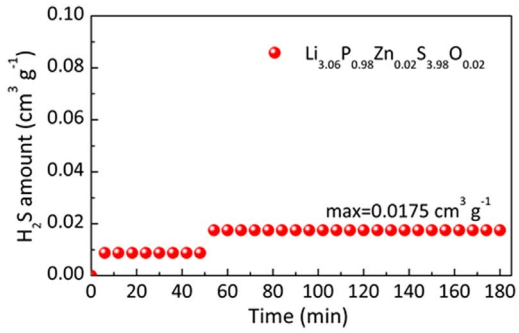

Fig. 9. The amount of H_2S generated from $Li_{3.06}P_{0.98}Zn_{0.02}S_{3.98}O_{0.02}$ when exposed in the humid air with different duration time.

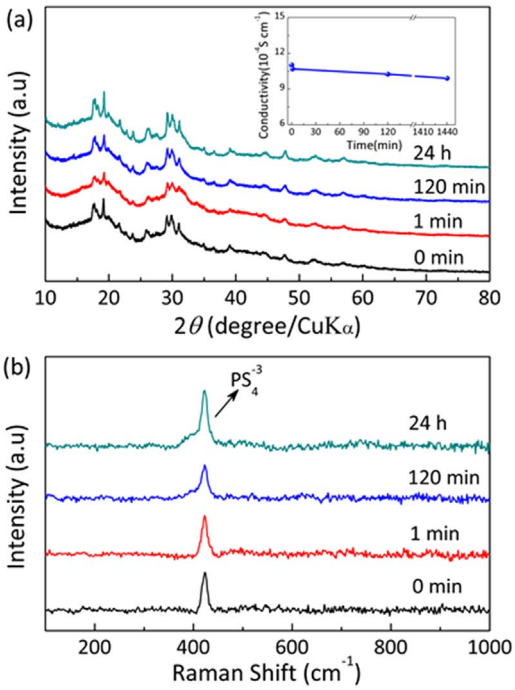

Fig. 10. The stability test of $Li_{3.06}P_{0.98}Zn_{0.02}S_{3.98}O_{0.02}$ conducted in chlorobenzene (a) the XRD and conductivity of samples with different soaking time; (b) the Raman results with different soaking time.

The stabilities of SEs in organic solvents were rarely reported by far, but they are crucial in processes such as coating, casting, roll-to-roll etc., and they are vital evaluation criteria of the application of SEs in LIBs production at massive scale. Therefore, the stability of $Li_{3.06}P_{0.98}Zn_{0.02}S_{3.98}O_{0.02}$ in organic solvent was studied in this paper. Chlorobenzene is the frequently-used and low-cost solvent. Herein, the $Li_{3.06}P_{0.98}Zn_{0.02}S_{3.98}O_{0.02}$ was soaked in chlorobenzene with 1:1 by volume for 1 min, 2 h, and 24 h, respectively. Then, they were dried and characterized by the XRD, EIS and Raman spectra.

The XRD patterns of unsoaked $Li_{3.06}P_{0.98}Zn_{0.02}S_{3.98}O_{0.02}$ sample and samples soaked for 1 min, 2 h, 24 h are demonstrated in Fig. 10a. No significant differences of peak positions and intensities could be observed among all these samples, suggesting its crystal structure almost remain the same after soaking. The inset in Fig. 10a shows that the ionic conductivity still maintained at the order of 10^{-3} S cm^{-1} after soaking for 24 h, and incline to remain constant as the soaking time increases. Fig. 10b illustrates the Raman spectra of $Li_{3.06}P_{0.98}Zn_{0.02}S_{3.98}O_{0.02}$ samples soaked for the different amount of time, showing the peak positions and intensities remain unchanged after soaking. This result well proves that $Li_{3.06}P_{0.98}Zn_{0.02}S_{3.98}O_{0.02}$ possess good chemical stability in chlorobenzene, which is beneficial to the coating process of lithium battery fabrication in a large scale. Thus, $Li_{3.06}P_{0.98}Zn_{0.02}S_{3.98}O_{0.02}$ has great potential as a SE material, which can be used in ASSLBs designs in a free standing form without modifying current battery fabrication processes.

3.7. Cell performance

LGPS exhibits a superior conductivity up to 1.2×10^{-2} S cm^{-1}, but it suffers from poor stability in the low voltage range as evidenced by CV and *ex-situ* XRD experiments, especially, the instablilty against lithium, which resulted in a severe capacity fading of the lithium metal batteries [4,44]. Therefore, ASSLBs with bi-layer electrolyte configuration was proposed [45]. The battery with such a structure exhibited better electrochemical performance than that of ones with a single electrolyte layer [46].

Herein, ASSLBs with bi-layer electrolytes were assembled, and

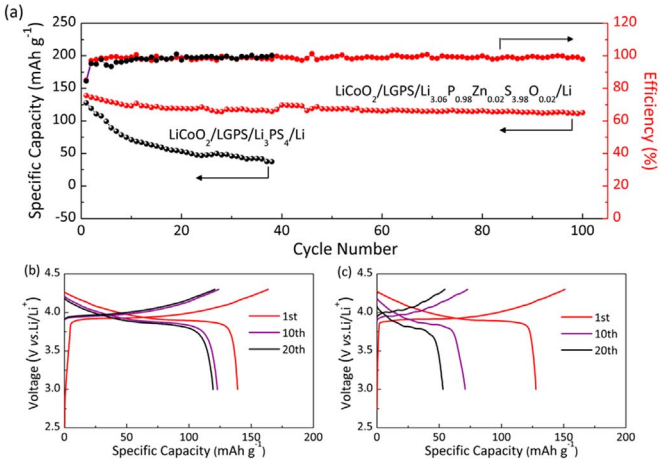

Fig. 11. (a) The cycling performance of the cell $LiCoO_2$/LGPS/$Li_{3.06}P_{0.98}Zn_{0.02}S_{3.98}O_{0.02}$/Li and $LiCoO_2$/LGPS/Li_3PS_4/Li; charge-discharge curves of (b) $LiCoO_2$/LGPS/$Li_{3.06}P_{0.98}Zn_{0.02}S_{3.98}O_{0.02}$/Li and (c) $LiCoO_2$/LGPS/Li_3PS_4/Li cells. The all-solid-state cells are cycled at 0.1 C (1 C = 120mAh g^{-1}) in the range of 3.0-4.3 V vs. Li/Li^+ at room temperature.

displayed an excellent cell performance, in which bi-layer electrolytes including the LGPS and $Li_{3.06}P_{0.98}Zn_{0.02}S_{3.98}O_{0.02}$ (or Li_3PS_4) were adapted in this work [45]. To be specific, the ASSLBs with $LiNbO_3$-coated $LiCoO_2$ and LGPS powder as cathode material, LGPS and $Li_{3.06}P_{0.98}Zn_{0.02}S_{3.98}O_{0.02}$ (or Li_3PS_4) as the bi-layer electrolytes and metallic Li foil as anode, and their cycling performances were tested at 0.1 C in the range of 3.0-4.3 V *vs.* Li/Li^+ at room temperature. Attractively, the $LiCoO_2$/LGPS/$Li_{3.06}P_{0.98}Zn_{0.02}S_{3.98}O_{0.02}$/Li cell delivers a high discharge capacity of 112.7 mAh g^{-1} with a high retention of 81.0% after 100 cycles, while the cell of $LiCoO_2$/LGPS/Li_3PS_4/Li displays an initial discharge capacity of 127.7 mAh g^{-1} at 0.1 C and only 37.7% capacity retention after 40 cycles at room temperature. The improved specific capacity and cycle life are attributed to the higher conductivity and superior stability against lithium of $Li_{3.06}P_{0.98}Zn_{0.02}S_{3.98}O_{0.02}$.

Galvanostatic charge-discharge curves (Fig. 11b) are used to show the running behavior of the ASSLBs. Both of $LiCoO_2$/LGPS/$Li_{3.06}P_{0.98}Zn_{0.02}S_{3.98}O_{0.02}$/Li (Fig. 11b) and $LiCoO_2$/LGPS/Li_3PS_4/Li (Fig. 11c) cells show only a small overpotential for initial charge and discharge curves. At the 10^{th} and 20^{th} of the charge-curve of the $LiCoO_2$/LGPS/$Li_{3.06}P_{0.98}Zn_{0.02}S_{3.98}O_{0.02}$/Li cell, an increase of the potential occurs, while an obvious larger potential appear at $LiCoO_2$/LGPS/Li_3PS_4/Li cell due to the preferably stability against lithium of $Li_{3.06}P_{0.98}Zn_{0.02}S_{3.98}O_{0.02}$. Furthermore, the EIS was applied to study the interfacial evolution of ASSLBs along cycling. Both of the Nyquist plots are composed of a depressed semicircle at the high frequency region and a straight line at the low frequency region in Fig. S2.

4. Conclusions

In this paper, a new sulfide electrolyte of $Li_{3.06}P_{0.98}Zn_{0.02}S_{3.98}O_{0.02}$ was successfully synthesized by aliovalent substitution of 2 mol% ZnO, in which partial P^{5+} is substituted by Zn^{2+}, and a part of S^{2-} is replaced by O^{2-}. Its electrochemical properties are examined systematically, and it presents a superior conductivity of 1.12×10^{-3} S cm^{-1}, 6 V electrochemical window, and good stability against lithium metal as well as outstanding stability in air. The improved mechanism of the ZnO dual-doped electrolyte has been analyzed and explained through theoretical calculations, which provided the theoretical basis for further enhancement of the chemical stability and conductivity of Li_3PS_4 materials. The ASSLB assembled with the bi-layer electrolytes shows an initial discharge capacity of 139.1 mAh g^{-1} at 0.1 C and a capacity retention of 81.0% after 100 cycles, which are better than that of $LiCoO_2$/$Li_{10}GeP_2S_{12}$/Li_3PS_4/Li cell (127.7 mAh g^{-1} at 0.1 C and 37.7% capacity retention after 60 cycles). Consequently, $Li_{3.06}P_{0.98}Zn_{0.02}S_{3.98}O_{0.02}$ has great potential in the application of ASSLBs.

Acknowledgements

This work was supported by funding from National Key R & D Program of China (Grant No. 2018YFB0905400), the Strategic Priority Program of the Chinese Academy of Sciences (Grant No. XDA09010201, XDA09010203), the National Natural Science Foundation of China (Grant No. 51502317, 51772321), Zhejiang Provincial Natural Science Foundation of China (Grant No. LQ16E020003, LY18E020018, LY18E030011, LD18E020004), National Key Research and Development Program of China (Grant No. 2016YFB0100105) and Youth Innovation Promotion Association of the Chinese Academy of Sciences (Grant No. 2017342, 2016005).

Appendix A. Supporting information

Supplementary data associated with this article can be found in the online version at doi:10.1016/j.ensm.2018.07.008.

References

[1] Y. Kato, S. Hori, T. Saito, K. Suzuki, M. Hirayama, A. Mitsui, M. Yonemura, H. Iba, R. Kanno, High-power all-solid-state batteries using sulfide superionic conductors, Nat. Energy 1 (2016) 16030–16036.
[2] P.G. Bruce, A. West, The A-C conductivity of polycrystalline LISICON, $Li_{2+2x}Zn_{1-x}GeO_4$, and a model for intergranular constriction resistances, J. Electrochem Soc. 130 (1983) 662–669.
[3] T. Hakari, M. Nagao, A. Hayashi, M. Tatsumisago, All-solid-state lithium batteries with Li_3PS_4 glass as active material, J. Power Sources 293 (2015) 721–725.
[4] N. Kamaya, K. Homma, Y. Yamakawa, M. Hirayama, R. Kanno, M. Yonemura, T. Kamiyama, Y. Kato, S. Hama, K. Kawamoto, A. Mitsui, A lithium superionic conductor, Nat. Mater. 10 (2011) 682–686.
[5] Y. Ren, K. Chen, R. Chen, T. Liu, Y. Zhang, C.-W. Nan, B. Vyas, Oxide electrolytes for lithium batteries, J. Am. Ceram. Soc. 98 (2015) 3603–3623.
[6] G.-y Adachi, Imanaka Nobuhito, Aono Hiromichi, Fast Li^+ conducting ceramic electrolytes, Adv. Mater. 8 (1996) 127–135.
[7] Y. Seino, M. Nakagawa, M. Senga, H. Higuchi, K. Takada, T. Sasaki, Analysis of the Structure and degree of crystallisation of $70Li_2S$–$30P_2S_5$ glass ceramic, J. Mater. Chem. A 3 (2015) 2756–2761.
[8] A. Hayashi, M. Tatsumisago, Invited paper: recent development of bulk-type solid-state rechargeable lithium batteries with sulfide glass-ceramic electrolytes, Electron. Mater. Lett. 8 (2012) 199–207.
[9] R. Kanno, M. Murayama, Lithium ionic conductor Thio-LISICON: the Li_2S-GeS_2-P_2S_5 system, J. Electrochem. Soc. 148 (2001) A742–A746.
[10] A. Hayashi, H. Muramatsu, T. Ohtomo, S. Hama, M. Tatsumisago, Improvement of chemical stability of Li_3PS_4 glass electrolytes by adding M_xO_y (M = Fe, Zn, and Bi) nanoparticles, J. Mater. Chem. A 1 (2013) 6320.
[11] J. Haruyama, K. Sodeyama, Y. Tateyama, Cation mixing properties toward Co Diffusion at the $LiCoO_2$ cathode/sulfide electrolyte interface in a solid-state battery, ACS Appl. Mater. Interfaces 9 (2017) 286–292.
[12] K. Takada, S. Nakano, T. Inada, A. Kajiyama, H. Sasaki, S. Kondo, M. Watanabe, Compatibility of lithium ion conductive sulfide glass with carbon-lithium electrode, J. Electrochem. Soc. 150 (2003) A274–A277.
[13] K. Takada, Solid-state lithium battery with graphite anode, Solid State Ion. 158 (2003) 269–274.
[14] T. Kobayashi, A. Yamada, R. Kanno, Interfacial reactions at electrode/electrolyte boundary in all solid-state lithium battery using inorganic solid electrolyte, Thio-LISICON, Electrochim. Acta 53 (2008) 5045–5050.
[15] H. Muramatsu, A. Hayashi, T. Ohtomo, S. Hama, M. Tatsumisago, Structural change of Li_2S–P_2S_5 sulfide solid electrolytes in the atmosphere, Solid State Ion. 182 (2011) 116–119.
[16] Y. Yang, Q. Wu, Y. Cui, Y. Chen, S. Shi, R.Z. Wang, H. Yan, Elastic properties, defect thermodynamics, electrochemical window, phase stability, and Li^+ mobility of Li_3PS_4: insights from first-principles calculations, ACS Appl. Mater. Interfaces 8 (2016) 25229–25242.
[17] J.E. Trevey, J.R. Gilsdorf, S.W. Miller, S.-H. Lee, Li_2S–Li_2O–P_2S_5 solid electrolyte for all-solid-state lithium batteries, Solid State Ion. 214 (2012) 25–30.
[18] T. Ohtomo, A. Hayashi, M. Tatsumisago, K. Kawamoto, Characteristics of the Li_2O–Li_2S–P_2S_5 glasses synthesized by the two-step mechanical milling, J. Non-Cryst. Solids . 364 (2013) 57–61.
[19] P. Lu, F. Ding, Z. Xu, J. Liu, X. Liu, Q. Xu, Study on (100-x)($70Li_2S$-$30P_2S_5$)-xLi_2ZrO_3 glass-ceramic electrolyte for all-solid-state lithium-ion batteries, J. Power Sources 356 (2017) 163–171.
[20] K. Minami, F. Mizuno, A. Hayashi, M. Tatsumisago, Structure and properties of the $70Li_2S{\cdot}(30-x)P_2S_5{\cdot}xP_2O_5$ oxysulfide glasses and glass–ceramics, J. Non-Cryst.

Solids . 354 (2008) 370–373.
[21] K. Minami, A. Hayashi, M. Tatsumisago, Electrical and electrochemical properties of the $70Li_2S\cdot(30-x)P_2S_5\cdot xP_2O_5$ glass-ceramic electrolytes, Solid State Ion. 179 (2008) 1282–1285.
[22] T. Ohtomo, F. Mizuno, A. Hayashi, K. Tadanaga, M. Tatsumisago, Electrical and electrochemical properties of $Li_2S–P_2S_5–P_2O_5$ glass–ceramic electrolytes, J. Power Sources 146 (2005) 715–718.
[23] Y.C. Tao, S.J. Chen, D. Liu, G. Peng, X.Y. Yao, X.X. Xu, Lithium superionic conducting oxysulfide solid electrolyte with excellent stability against lithium metal for all-solid-state cells, J. Electrochem. Soc. 163 (2016) A96–A101.
[24] B.X. Huang, X.Y. Yao, Z. Huang, Y. Guan, Y. Jin, X.X. Xu, Li_3PO_4-doped $Li_7P_3S_{11}$ glass-ceramic electrolytes with enhanced lithium ion conductivities and application in all-solid-state batteries, J. Power Sources 284 (2015) 206–211.
[25] J. Kim, Y. Yoon, M. Eom, D. Shin, Characterization of amorphous and crystalline $Li_2S–P_2S_5–P_2Se_5$ solid electrolytes for all-solid-state lithium ion batteries, Solid State Ion. 225 (2012) 626–630.
[26] G. Sahu, Z. Lin, J. Li, Z. Liu, N. Dudney, C. Liang, Air-stable, high-conduction solid electrolytes of arsenic-substituted Li_4SnS_4, Energy Environ. Sci. 7 (2014) 1053–1058.
[27] T. Ohtomo, A. Hayashi, M. Tatsumisago, K. Kawamoto, Glass electrolytes with high ion conductivity and high chemical stability in the system LiI-Li_2O-Li_2S-P_2S_5, Electrochemistry 81 (2013) 428–431.
[28] G. Kresse, J. Furthmüller, Efficiency of Ab-initio total energy calculations for metals and semiconductors using a plane-wave basis set, Comp. Mater. Sci. 6 (1996) 15–50.
[29] P.E. Blöchl, Projector augmented-wave method, Phys. Rev. B 50 (1994) 17953–17979.
[30] J.P. Perdew, K. Burke, M. Ernzerhof, Generalized gradient approximation made simple, Phys. Rev. Lett. 77 (1996) 3865–3868.
[31] S. Adams, R.P. Rao, High power lithium ion battery materials by computational design, Phys. Status Solidi A 208 (2011) 1746–1753.
[32] K. Momma, F. Izumi, VESTA 3 for Three-dimensional visualization of crystal, volumetric and morphology data, J. Appl. Crystallogr. 44 (2011) 1272–1276.
[33] J.C. Bachman, S. Muy, A. Grimaud, H.H. Chang, N. Pour, S.F. Lux, O. Paschos, F. Maglia, S. Lupart, P. Lamp, L. Giordano, Y. Shao-Horn, Inorganic solid-state electrolytes for lithium batteries: mechanisms and properties governing ion conduction, Chem. Rev. 116 (2016) 140–162.
[34] Z. Zhang, S. Chen, J. Yang, J. Wang, L. Yao, X. Yao, P. Cui, X. Xu, Interface re-engineering of $Li_{10}GeP_2S_{12}$ electrolyte and lithium anode for all-solid-state lithium batteries with ultralong cycle life, ACS Appl. Mater. Interfaces 10 (2018) 2556–2565.
[35] X. Yao, N. Huang, F. Han, Q. Zhang, H. Wan, J.P. Mwizerwa, C. Wang, X. Xu, High-performance all-solid-state lithium-sulfur batteries enabled by amorphous sulfur-coated reduced graphene oxide cathodes, Adv. Energy Mater. 7 (2017) 1602923.
[36] N. Ohta, K. Takada, I. Sakaguchi, L. Zhang, R. Ma, K. Fukuda, M. Osada, T. Sasaki, $LiNbO_3$ -Coated $LiCoO_2$ as cathode material for all-solid-state lithium secondary batteries, Electrochem. Commun. 9 (2007) 1486–1490.
[37] D.L. Zhang, Processing of advanced materials using high-energy mechanical, Milling, Prog. Mater. Sc. 49 (2004) 537–560.
[38] K. Homma, M. Yonemura, T. Kobayashi, M. Nagao, M. Hirayama, R. Kanno, Crystal Structure and phase transitions of the lithium ionic conductor Li_3PS_4, Solid State Ion. 182 (2011) 53–58.
[39] F. Mizuno, A. Hayashi, K. Tadanaga, M. Tatsumisago, High lithium ion conducting glass-ceramics in the system $Li_2S–P_2S_5$, Solid State Ion. 177 (2006) 2721–2725.
[40] N.D. Lepley, N.A.W. Holzwarth, Y.A. Du, Structures, Li^+ mobilities, and interfacial properties of solid electrolytes Li_3PS_4 and Li_3PO_4 from first principles, Phys. Rev. B 88 (2013).
[41] X. Wang, R. Xiao, H. Li, L. Chen, Oxygen-driven transition from two-dimensional to three-dimensional transport behaviour in Beta-Li_3PS_4 electrolyte, Phys. Chem. Chem. Phys. 18 (2016) 21269–21277.
[42] Y. Seino, T. Ota, K. Takada, A. Hayashi, M. Tatsumisago, A sulphide lithium super ion conductor is superior to liquid ion conductors for use in rechargeable batteries, Energy Environ. Sci. 7 (2014) 627–631.
[43] R. Xiao, H. Li, L. Chen, Candidate structures for inorganic lithium solid-state electrolytes identified by high-throughput bond-valence calculations, J. Mater. 1 (2015) 325–332.
[44] B.R. Shin, Y.J. Nam, D.Y. Oh, D.H. Kim, J.W. Kim, Y.S. Jung, Comparative study of TiS_2 /Li-In all-solid-state lithium batteries using glass-ceramic Li_3PS_4 and $Li_{10}GeP_2S_{12}$ solid electrolytes, Electrochim. Acta 146 (2014) 395–402.
[45] J.E. Trevey, Y.S. Jung, S.-H. Lee, High lithium ion conducting $Li_2S–GeS_2–P_2S_5$ glass–ceramic solid electrolyte with sulfur additive for all solid-state lithium secondary batteries, Electrochim. Acta 56 (2011) 4243–4247.
[46] H.L. Wan, G. Peng, X.Y. Yao, J. Yang, P. Cui, X.X. Xu, Cu_2ZnSnS_4/graphene nanocomposites for ultrafast, long life all-solid-state lithium batteries using lithium metal anode, Energy Storage Mater. 4 (2016) 59–65.

Gaozhan Liu received her Bachelor's degree in Materials Science and Engineering at Wuhan University of Technology in 2016. Now, she is pursuing her Ph.D. degree at Ningbo Institute of Materials Technology and Engineering (NIMTE), Chinese Academy of Sciences. Her research focuses on sulfide electrolyte materials of all-solid-state lithium batteries.

Dongjiu Xie is currently a research assistant in Ningbo Institute of Materials Technology and Engineering (NIMTE), Chinese Academy of Sciences. He obtained his Bacherlor's degree from Yanshan University in 2013 and Master's Degree in 2016 at Fujian Normal University & Fujian Institute of Research on the Structure of Matter, Chinese Academy of Sciences. His interests are mainly on sulfide electrolytes and their application in all-solid-state lithium batteries.

Xuelong Wang is currently pursuing his Ph.D. degree at Institute of Physics, Chinese Academy of Sciences (IoP, CAS). He received his Bachelor's degree in Physics at Renmin University of China in 2013. His research interests are mainly focused on modeling and simulation of Li-ion battery involved materials, including First-principle simulation and meso-scale modeling.

Xiayin Yao is a professor at Ningbo Institute of Materials Technology and Engineering (NIMTE), Chinese Academy of Sciences. He received Ph.D in materials physics and chemistry from Institute of Solid State Physics and NIMTE, Chinese Academy of Sciences, P. R. China in 2009. After that, he joined NIMTE and worked there until now. During 2012-2014, he was a research fellow in Hanyang University, S. Korea and Nanyang Technological University, Singapore. Up to now, he has published over 60 peer-reviewed journal papers and applied more than 20 Chinese patents. His major interests include developing solid state electrolytes with high ionic conductivities and solid-state lithium-sulfur batteries as well as solid-state sodium batteries.

Shaojie Chen is an associate professor in Ningbo Institute of Materials Technology and Engineering (NIMTE), Chinese Academy of Sciences. He got his Ph.D degree from Northwestern Polytechnical University in 2012. During 2012-2014, he held a post-doctoral scholarship in the NIMTE, Chinese Academy of Sciences. After that, he joined NIMTE and worked there until now. His research work focuses on the development of sulfide electrolytes, hybrid electrolytes and their applications in solid-state lithium metal batteries. To date, he has published more than 20 papers, and filed more than 10 patents.

Ruijuan Xiao is an Associate Professor in Key Laboratory For Renewable Energy, Institute of Physics, Chinese Academy of Sciences, Beijing, China. Before joining the faculty of Institute of Physics in 2010, she had conducted Post Doc. studies in IFW Dresden, Germany since 2007. Her recent research focuses on theoretical simulations on lithium-ion battery materials, including the investigations on the (de)lithiation mechanisms, kinetic properties, electronic conductivities of battery materials, and the relationships between the basic properties of materials and the performance of the batteries.

Hong Li is a professor in Institute of Physics, Chinese academy of Science. His research interest include fundamental researches in batteries, such as transport of ions and electrons, size effect, interface phenomena, structure evolution as well as application researches, including high energy density Li-ion batteries using Si based anode, solid lithium batteries and their failure analysis. He is leading a CAS SPRP "Battery for EV" 5-year program and serve as a committee member for Advanced Energy in Ministry of Science and Technology of China since 2012.

Xiaoxiong Xu is an adjunct professor in the Ningbo Institute of Materials Technology and Engineering (NIMTE), Chinese Academy of Sciences. He got his Ph.D degree form Shanghai Institute of Ceramics, Chinese Academy of Sciences (SICCAS) in 2007. Then, he joined in National Institute for Materials Science (NIMS), Japan as a postdoctoral fellow from 2007 to 2011. Prof. Xu's research work focuses on all-solid-state lithium batteries with high performance and solid-state lithium-sulfur batteries. To date, he has published more than 60 peer-review journal papers and applied for 30 patents. He is the recipient of the outstanding research award from Chinese Ceramic Society.